Chapter 2

Angular Spectrum Representation of Optical Fields

The angular spectrum representation is a mathematical technique to describe optical fields in homogeneous media. Optical fields are described as a superposition of plane waves and evanescent waves which are physically intuitive solutions of Maxwell's equations. The angular spectrum representation is found to be a very powerful method for the description of laser beam propagation and light focusing. Furthermore, in the paraxial limit, the angular spectrum representation becomes identical with the framework of Fourier optics which extents its importance even further. In the subsequent sections we will apply the angular spectrum representation to gain an understanding of the limits of farfield optics.

2.1 Basic Formalism

Under angular spectrum representation we understand the series expansion of an arbitrary field in terms of plane waves with variable amplitudes and propagation directions. Assume we know the electric field $\mathbf{E}(\mathbf{r})$ at any point $\mathbf{r} = (x, y, z)$ in space. For example, $\mathbf{E}(\mathbf{r})$ can be the solution of an optical scattering problem as shown in Fig. 2.1 for which $\mathbf{E} = \mathbf{E}_{inc} + \mathbf{E}_{scatt}$. In the angular spectrum picture, we draw an arbitrary axis z and consider the field $\mathbf{E}$ in a plane $z = const$ transverse to the chosen axis. In this plane we can evaluate the two dimensional Fourier transform of the field $\mathbf{E}$ as

$$\hat{\mathbf{E}}(k_x, k_y; z) \;=\; \frac{1}{2\pi} \iint_{-\infty}^{\infty} \mathbf{E}(x, y, z)\; \mathrm{e}^{-i[k_x x + k_y y]}\; dx\, dy\;, \tag{2.1}$$

where x, y are the Cartesian transverse coordinates and k_x, k_y the corresponding spatial frequencies or reciprocal coordinates. Similarly, the inverse Fourier transform reads as

$$\mathbf{E}(x, y, z) \;=\; \frac{1}{2\pi} \iint_{-\infty}^{\infty} \hat{\mathbf{E}}(k_x, k_y;\, z)\; \mathrm{e}^{\,i\,[k_x\, x \,+\, k_y\, y]}\; dk_x\, dk_y \;. \tag{2.2}$$

Notice, that in the notation of Eqs. 2.1 and 2.2 the field $\mathbf{E} = (E_x, E_y, E_z)$ and its Fourier transform $\hat{\mathbf{E}} = (\hat{E}_x, \hat{E}_y, \hat{E}_z)$ represent vectors. Thus, the Fourier integrals hold separately for each vector component.

So far we have made no requirements about the field $\mathbf{E}$, but we will assume that in the transverse plane the medium is homogeneous, isotropic, linear and source-free. Then, a time-harmonic, optical field with angular frequency ω has to satisfy the vector Helmholtz equation

$$(\nabla^2 + k^2)\; \mathbf{E}(\mathbf{r}) \;=\; 0 \;, \tag{2.3}$$

where k is determined by $k = (\omega/c)\, n$ and $n = \sqrt{\mu\varepsilon}$ is the index of refraction. In order to get the time-dependent field $\mathbf{E}(\mathbf{r}, t)$ we use the convention

$$\mathbf{E}(\mathbf{r}, t) \;=\; Re\{\mathbf{E}(\mathbf{r})\, \mathrm{e}^{-i\omega t}\} \;. \tag{2.4}$$

Inserting the Fourier representation of $\mathbf{E}(\mathbf{r})$ (Eq. 2.2) into the Helmholtz equation and defining

$$k_z \;\equiv\; \sqrt{(k^2 - k_x^2 - k_y^2)} \qquad with \quad Im\{k_z\} \geq 0 \;, \tag{2.5}$$

we find that the Fourier spectrum $\hat{\mathbf{E}}$ evolves along the z-axis as

$$\hat{\mathbf{E}}(k_x, k_y;\, z) \;=\; \hat{\mathbf{E}}(k_x, k_y;\, 0)\; \mathrm{e}^{\pm i\, k_z\, z} \;. \tag{2.6}$$

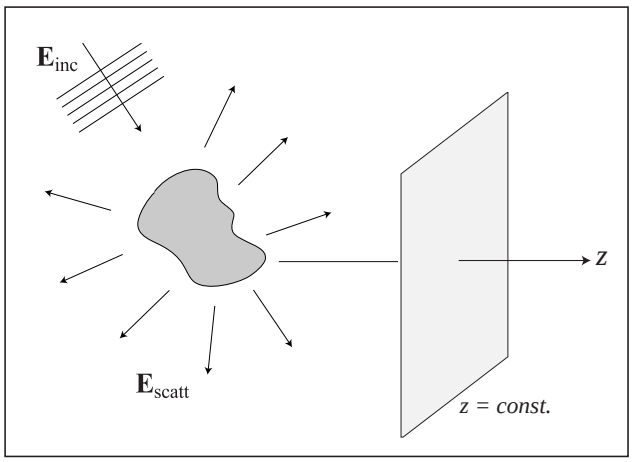

Figure 2.1: In the angular spectrum representation the fields are evaluated in planes ($z = const$) perpendicular to an arbitrarily chosen axis z.

The '±' sign specifies that we have two solutions that need to be superimposed: the '+' sign refers to a wave propagating into the half-space $z > 0$ whereas the '−' sign denotes a wave propagating into $z < 0$. Eq. 2.6 tells us that the Fourier spectrum of $\mathbf{E}$ in an arbitrary *image plane*) located at $z = const$ can be calculated by multiplying the spectrum in the *object plane* at $z = 0$ by the factor $exp(\pm i\, k_z\, z)$. This factor is called *propagator* in reciprocal space. In Eq. 2.5 we defined that the square root leading to k_z renders a result with positive imaginary part. This ensures that the solutions remain finite for $z \to \pm\infty$. Inserting the result of Eq. 2.6 into Eq. 2.2 we finally find for arbitrary z

$$\boxed{\mathbf{E}(x, y, z) \;=\; \frac{1}{2\pi} \iint_{-\infty}^{\infty} \hat{\mathbf{E}}(k_x, k_y; 0)\; \mathrm{e}^{\,i\,[k_x\, x \,+\, k_y\, y \,\pm\, k_z\, z]}\; dk_x\, dk_y} \tag{2.7}$$

which is known as the *angular spectrum representation*. In a similar way, we can also represent the magnetic field $\mathbf{H}$ by an angular spectrum as

$$\mathbf{H}(x, y, z) \;=\; \frac{1}{2\pi} \iint_{-\infty}^{\infty} \hat{\mathbf{H}}(k_x, k_y; 0)\; \mathrm{e}^{\,i\,[k_x\, x \,+\, k_y\, y \,\pm\, k_z\, z]}\; dk_x\, dk_y \;, \tag{2.8}$$

By using Maxwell's equation $\mathbf{H} = (i\omega\mu\mu_o)^{-1}\,(\nabla \times \mathbf{E})$ we find the following relationship between the Fourier spectra $\hat{\mathbf{E}}$ and $\hat{\mathbf{H}}$

$$\begin{aligned}
\hat{H}_x &= Z_{\mu\epsilon}^{-1}\,[(k_y/k)\,\hat{E}_z - (k_z/k)\,\hat{E}_y]\;, \\
\hat{H}_y &= Z_{\mu\epsilon}^{-1}\,[(k_z/k)\,\hat{E}_x - (k_x/k)\,\hat{E}_z]\;, \\
\hat{H}_z &= Z_{\mu\varepsilon}^{-1}\,[(k_x/k)\,\hat{E}_y - (k_y/k)\,\hat{E}_x]\;,
\end{aligned} \tag{2.9}$$

where $Z_{\mu\varepsilon} = \sqrt{(\mu_o\mu)/(\varepsilon_o\varepsilon)}$ is the wave impedance of the medium. Although the angular spectra of $\mathbf{E}$ and $\mathbf{H}$ fulfill Helmholtz equation they are not yet rigorous solutions of Maxwell's equations. We still have to require that the fields are divergence free, i.e. $\nabla\cdot\mathbf{E} = 0$ and $\nabla\cdot\mathbf{H} = 0$. These conditions restrict the k vector to directions perpendicular to the field vectors ($\mathbf{k}\cdot\mathbf{E} = \mathbf{k}\cdot\mathbf{H} = 0$).

For the case of a purely dielectric medium with no losses the index of refraction n is a real and positive quantity. The wavenumber k_z is then either real or imaginary and turns the factor $exp(\pm i\, k_z\, z)$ into an oscillatory or exponentially decaying function. For a certain $(k_x,\, k_y)$ pair we then find two different characteristic solutions

$$\boxed{\begin{aligned}
Plane\,waves: &\quad \mathrm{e}^{\,i\,[k_x\, x \,+\, k_y\, y]}\;\mathrm{e}^{\,\pm i\,|k_z|\,z}, &\quad k_x^2 + k_y^2 \le k^2 \\
Evanescent\,waves: &\quad \mathrm{e}^{\,i\,[k_x\, x \,+\, k_y\, y]}\;\mathrm{e}^{\,-|k_z|\,|z|}, &\quad k_x^2 + k_y^2 > k^2
\end{aligned}} \tag{2.10}$$

Hence, we find that the angular spectrum is indeed a superposition of *plane waves* and *evanescent waves*. Plane waves are oscillating functions in z and are restricted by the condition $k_x^2 + k_y^2 \le k^2$. On the other hand, for $k_x^2 + k_y^2 > k^2$ we encounter evanescent waves with an exponential decay along the z axis. Fig. 2.2 shows that the larger the angle between the

k-vector and the z axis is, the larger the oscillations in the transverse plane will be. A plane wave propagating in direction of z has no oscillations in the transverse plane ($k_x^2 + k_y^2 = 0$), whereas, in the other limit, a plane wave propagating at a right angle to z shows the highest spatial oscillations in the transverse plane ($k_x^2 + k_y^2 = k^2$). Even higher spatial frequencies are achieved by evanescent waves. In principle, an infinite bandwidth of spatial frequencies can be achieved. However, the higher the spatial frequencies of an evanescent wave are, the stronger the field decay along the z axis will be. Therefore, practical limitations make the bandwidth finite.

So far we know from Eq. 2.6 how the Fourier spectrum of **E** propagates along the z axis. Let us now determine how the fields themselves evolve. For this purpose we denote the transverse coordinates in the object plane at $z = 0$ as (x', y') and in the image plane at $z = const$ as (x, y). The fields in the image plane are described by the angular spectrum (Eq. 2.7). We just have to express the Fourier spectrum $\hat{\mathbf{E}}(k_x, k_y; 0)$ in terms of the fields in the object plane. Similar to Eq. 2.1 this Fourier spectrum can be represented as

$$\hat{\mathbf{E}}(k_x, k_y; 0) \;=\; \frac{1}{2\pi} \iint_{-\infty}^{\infty} \mathbf{E}(x', y', 0)\; \mathrm{e}^{-i[k_x x' + k_y y']}\; dx'\, dy' \;. \tag{2.11}$$

After inserting into Eq. 2.6 we find the following expression for the field **E** in the image plane $z = const$.

$$\mathbf{E}(x, y, z) \;=\; \frac{1}{4\pi^2} \iint_{-\infty}^{\infty} \mathbf{E}(x', y'; 0) \iint_{-\infty}^{\infty} \mathrm{e}^{i[k_x (x - x') + k_y (y - y') \pm k_z z]}\; dx'\, dy' dk_x\, dk_y \;. \tag{2.12}$$

This equation describes an invariant filter with the following impulse response (*propagator*

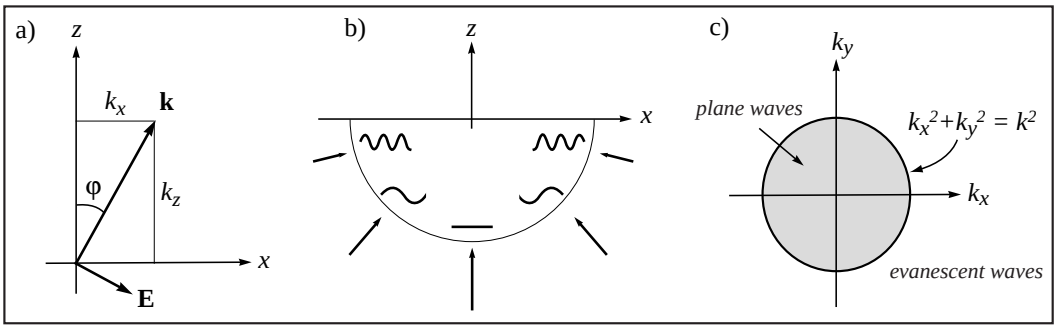

Figure 2.2: a) Representation of a plane wave propagating at an angle φ to the z axis. b) Illustration of the transverse spatial frequencies of plane waves incident from different angles. The transverse wavenumber $(k_x^2 + k_y^2)^{1/2}$ depends on the angle of incidence and is limited to the interval $[0\,..\,k]$. c) The transverse wavenumbers k_x, k_y of plane waves are restricted to a circular area with radius k. Evanescent waves fill the space outside the circle.

in direct space)

$$H(x-x',\,y-y';\,z) \;=\; \frac{1}{4\pi^2}\iint_{-\infty}^{\infty} \mathrm{e}^{i\,[k_x(x-x')\,+\,k_y(y-y')\,\pm\,k_z\,z]}\;dk_x\,dk_y\;. \tag{2.13}$$

The field at $z = const.$ is represented by the convolution of H with the field at $z=0$. The filter H is an oscillating function for $(k_x^2+k_y^2) < k^2$ and an exponentially decreasing function for $(k_x^2+k_y^2) > k^2$. Thus, if the image plane is sufficiently separated from the object plane, the contribution of the decaying parts (evanescent waves) is zero and the integration can be reduced to the circular area $(k_x^2+k_y^2) < k^2$. In other words, the image at z is a *low pass filtered* representation of the original field at $z=0$. The spatial frequencies $(k_x^2+k_y^2) > k^2$ of the original field are filtered out during propagation and the information on the high spatial variations gets lost. Hence, there is always a loss of information on the way of propagation from near- to far-field and only structures with lateral dimensions larger than

$$\Delta x \;\approx\; \frac{1}{k} = \frac{\lambda}{2\pi n} \tag{2.14}$$

can be imaged with sufficient accuracy. In general, higher resolution can be obtained by a higher index of refraction of the embodying system (substrate, lenses, etc.) or by shorter wavelengths. Theoretically, resolutions down to a few nanometers can be achieved by using far-ultraviolet radiation or X-rays. However, X-rays do cause damage to many samples. Furthermore, they are limited by the poor quality of lenses and do not provide the wealth of information of optical frequencies. The central idea of *near-field optics* is to increase the bandwidth of spatial frequencies by retaining a part of the evanescent components of the source fields.

2.2 Paraxial approximation of optical fields

In many optical problems the light fields propagate along a certain direction z and spread out only slowly in the transverse direction. Examples are laser beam propagation or optical waveguide applications. In these examples the wavevectors $\mathbf{k} = (k_x, k_y, k_z)$ in the angular spectrum representation are almost parallel to the z axis and the transverse wavenumbers (k_x, k_y) are small compared to k. We can then expand the square root of Eq. 2.5 in a series as

$$k_z \;=\; k\,\sqrt{1-(k_x^2+k_y^2)/k^2} \;\approx\; k \;-\; \frac{(k_x^2+k_y^2)}{2\,k}\;, \tag{2.15}$$

This approximation considerably simplifies the analytical integration of the Fourier integrals. In the following we shall apply the paraxial approximation to find a description for weakly focused laser beams.

2.2.1 Weakly focused laser beams

We consider a fundamental laser beam with a linearly polarized, Gaussian field distribution in the beam waist

$$\mathbf{E}(x',y',0) \;=\; \mathbf{E}_o\,\mathrm{e}^{-\frac{x'^2+y'^2}{w_o^2}}\;, \tag{2.16}$$

where $\mathbf{E}_o$ is a constant field vector in the transverse (x,y) plane. We have chosen $z = 0$ at the beam waist. The parameter w_o denotes the beam waist radius. We can calculate the Fourier spectrum at $z = 0$ as[1]

$$\begin{aligned}\hat{\mathbf{E}}(k_x, k_y; 0) &= \frac{1}{2\pi} \iint_{-\infty}^{\infty} \mathbf{E}_o \, \mathrm{e}^{-\frac{x'^2+y'^2}{w_o^2}} \, \mathrm{e}^{-i[k_x x' + k_y y']} \, dx' \, dy' \\ &= \mathbf{E}_o \, \frac{w_o^2}{2} \, \mathrm{e}^{-(k_x^2+k_y^2)\frac{w_o^2}{4}}, \end{aligned} \tag{2.17}$$

which is again a Gaussian function. We now insert this spectrum into the angular spectrum representation Eq. 2.7 and replace k_z by its paraxial expression in Eq. 2.15

$$\mathbf{E}(x, y, z) = \mathbf{E}_o \, \frac{w_o^2}{4\,\pi} \, \mathrm{e}^{i\,k\,z} \iint_{-\infty}^{\infty} \mathrm{e}^{-(k_x^2+k_y^2)(\frac{w_o^2}{4}+\frac{i\,z}{2\,k})} \, \mathrm{e}^{i[k_x\,x + k_y\,y]} \, dk_x \, dk_y \, , \tag{2.18}$$

This equation can be integrated and gives as a result the familiar paraxial representation of a Gaussian beam

$$\mathbf{E}(x, y, z) = \frac{\mathbf{E}_o \, \mathrm{e}^{i\,k\,z}}{(1 + 2\,i\,z/k w_o^2)} \, \mathrm{e}^{-\frac{(x^2+y^2)}{w_o^2}\frac{1}{(1+2\,i\,z/k\,w_o^2)}} \, . \tag{2.19}$$

To get a better feeling for a paraxial Gaussian beam we set $\rho^2 = x^2 + y^2$, define a new parameter z_o as

$$z_o = \frac{k\,w_o^2}{2} \, , \tag{2.20}$$

[1] $\int \exp(-ax^2 + ibx)\,dx = \sqrt{\pi/a}\,\exp(-b^2/4a)$ and $\int x\exp(-ax^2+ibx)\,dx = ib\sqrt{\pi}\,\exp(-b^2/4a)/(2a^{3/2})$

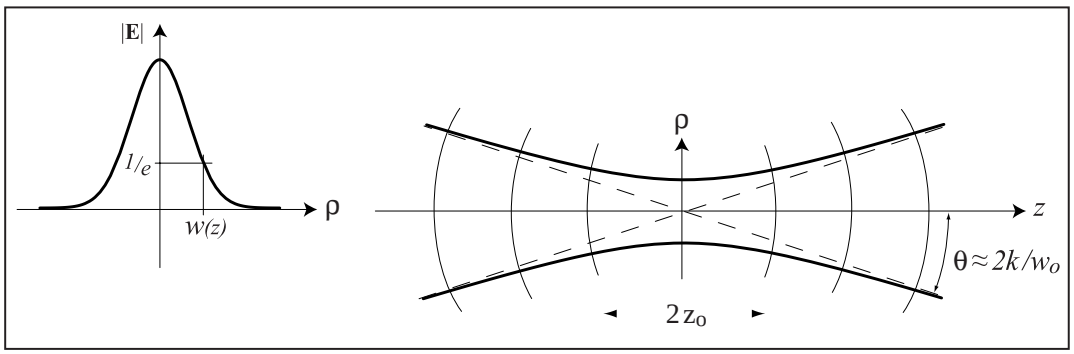

Figure 2.3: Illustration and main characteristics of a paraxial Gaussian beam. The beam has a Gaussian field distribution in the transverse plane. The surfaces of constant field strength form a hyperboloid along the z-axis.

and rewrite Eq. 2.19 as

$$\boxed{\mathbf{E}(\rho, z) \;=\; \mathbf{E}_o \,\frac{w_o}{w(z)}\, \mathrm{e}^{-\frac{\rho^2}{w^2(z)}}\, \mathrm{e}^{i[k\,z - \eta(z) + k\rho^2/2R(z)]}} \tag{2.21}$$

with the following abbreviations

$$\begin{aligned} w(z) &= w_o\,(1 + z^2/z_o^2)^{1/2} \qquad \textit{beam waist} \\ R(z) &= z\,(1 + z_o^2/z^2) \qquad \textit{wavefront radius} \\ \eta(z) &= \arctan z/z_o \qquad \textit{phase correction} \end{aligned} \tag{2.22}$$

The transverse size of the beam is usually defined by the value of $\rho = \sqrt{x^2 + y^2}$ for which the electric field amplitude is decayed to a value of $1/\mathrm{e}$ of its center value

$$|\mathbf{E}(x, y, z)| \,/\, |\mathbf{E}(0, 0, z)| \;=\; 1/\mathrm{e}\;. \tag{2.23}$$

It can be shown, that the surface defined by this equation is a hyperboloid whose asymptotes enclose an angle

$$\theta \;=\; \frac{2}{k\,w_o} \tag{2.24}$$

with the z axis. From this equation we can directly find the correspondence between the numerical aperture ($NA \;=\; n\,\sin\theta$) and the beam angle as $NA \approx 2n/kw_o$. Here we used the fact that in the paraxial approximation, θ is restricted to small beam angles. Another property of the paraxial Gaussian beam is that close to the focus, the beam stays roughly collimated over a distance $2z_o$. z_o is called the *Rayleigh range* and denotes the distance from the beam waist to where the spot has increased by a factor of $\sqrt{2}$. It is important to notice that along the z axis ($\rho = 0$) the phases of the beam deviate from those of a plane wave. If at $z \to -\infty$ the beam was in phase with a reference plane wave, then at $z \to +\infty$ the beam will be exactly out of phase with the reference wave. This phase shift is called *Gouy phase shift* and has practical implications in nonlinear confocal microscopy [1]. The 180° phase change happens gradually as the beam propagates through its focus. The phase variation is described by the factor $\eta(z)$ in Eq. 2.22. The tighter the focus the faster the phase variation will be.

A qualitative picture of a paraxial Gaussian beam and some of its characteristics are shown in Fig. 2.3 and more detailed descriptions can be found in other textbooks Ref. [2, 3]. It is important to notice that once the paraxial approximation is introduced, the field $\mathbf{E}$ does not fulfill Maxwell's equations anymore. The error becomes larger the smaller the beam waist radius w_o is. When w_o becomes comparable to the reduced wavelength λ/n we have to include higher order terms in the expansion of k_z in Eq. 2.15. However, the series expansion converges very badly for strongly focused beams and one needs to find a more accurate description. We shall return to this topic at a later stage.

2.3 Polarized electric and polarized magnetic fields

Any propagating optical field can be split into a polarized electric (PE) and a polarized magnetic (PM) field

$$\mathbf{E} = \mathbf{E}^{PE} \;+\; \mathbf{E}^{PM}\;. \tag{2.25}$$

For a PE field, the electric field is linearly polarized in the transverse plane. Similarly, for a PM field the magnetic field is linearly polarized in the transverse plane. Let us first consider a PE field for which we can choose $\mathbf{E}^{PE} = (E_x, 0, E_z)$. Requiring that the field is divergence free ($\nabla \cdot \mathbf{E}^{PE} = 0$) we find that

$$\hat{E}_z(k_x, k_y; 0) = -\frac{k_x}{k_z}\hat{E}_x(k_x, k_y; 0) , \tag{2.26}$$

which allows us to express the fields $\mathbf{E}^{PE}, \mathbf{H}^{PE}$ in the form

$$\mathbf{E}^{PE}(x,y,z) = \frac{1}{2\pi}\iint_{-\infty}^{\infty}\hat{E}_x(k_x, k_y; 0)\,\frac{1}{k_z}[k_z\mathbf{n}_x - k_x\mathbf{n}_z]\,\mathrm{e}^{i[k_x x + k_y y \pm k_z z]}\,dk_x\,dk_y , \tag{2.27}$$

$$\mathbf{H}^{PE}(x,y,z) = \frac{1}{2\pi Z_{\mu\varepsilon}}\iint_{-\infty}^{\infty}\hat{E}_x(k_x, k_y; 0)\,\frac{1}{kk_z}[-k_x k_y\mathbf{n}_x + (k_x^2 + k_z^2)\mathbf{n}_y - k_y k_z\mathbf{n}_z]\,\mathrm{e}^{i[k_x x + k_y y \pm k_z z]}\,dk_x\,dk_y , \tag{2.28}$$

where $\mathbf{n}_x$, $\mathbf{n}_y$, $\mathbf{n}_z$ are unit vectors along the x, y, z axes. To derive $\mathbf{H}^{PE}$ we used the relations in Eq. 2.9.

To derive the corresponding PM fields we require that $\mathbf{H}^{PM} = (0, H_y, H_z)$. After following the same procedure as before one finds that in the PM solution the expressions for the electric and magnetic fields are simply interchanged

$$\mathbf{E}^{PM}(x,y,z) = \frac{Z_{\mu\varepsilon}}{2\pi}\iint_{-\infty}^{\infty}\hat{H}_y(k_x, k_y; 0)\,\frac{1}{kk_z}[(k_y^2 + k_z^2)\mathbf{n}_x - k_x k_y\mathbf{n}_y + k_x k_z\mathbf{n}_z]\,\mathrm{e}^{i[k_x x + k_y y \pm k_z z]}\,dk_x\,dk_y , \tag{2.29}$$

$$\mathbf{H}^{PM}(x,y,z) = \frac{1}{2\pi}\iint_{-\infty}^{\infty}\hat{H}_y(k_x, k_y; 0)\,\frac{1}{k_z}[k_z\mathbf{n}_y - k_y\mathbf{n}_z]\,\mathrm{e}^{i[k_x x + k_y y \pm k_z z]}\,dk_x\,dk_y . \tag{2.30}$$

It is straight forward to demonstrate that in the paraxial limit the PE and PM solutions are identical. In this case they become identical with a TEM solution.

The decomposition of an arbitrary optical field into a PE and a PM field has been achieved by setting one transverse field component to zero. The procedure is similar to the commonly encountered decomposition into transverse electric (TE) and transverse magnetic (TM) fields for which one longitudinal field component is set to zero (see Problem 2.4).

2.3.1 Rigorous description of Gaussian beams

In the paraxial approximation the Gaussian beam is a TEM wave, i.e. simultaneously a PE and a PM wave. Therefore, the magnetic field has the same form as the electric field and its field vector is perpendicular to the propagation direction z and the field $\mathbf{E}$. If we assume that a Gaussian beam is characterized by having a Gaussian field distribution at the beam waist we can apply the angular spectrum framework to generalize the results in Section 2.2.1. However, depending whether we assume a Gaussian distribution for the electric or magnetic

field we arrive at PE or PM solutions. Let us first discuss the PE beam for which we require a Gaussian field distribution at the beam waist (c.f. Eq. 2.16). We choose the x axis of our coordinate system along the constant field vector $\mathbf{E}_o$, i.e. $\mathbf{E}_o = E_o\,\mathbf{n}_x$. The corresponding Fourier spectrum has been determined in Eq. 2.17 as

$$\hat{E}_x(k_x, k_y; 0) \;=\; E_o\,\frac{w_o^2}{2}\,\mathrm{e}^{-(k_x^2+k_y^2)\frac{w_o^2}{4}}, \tag{2.31}$$

This spectrum can now be inserted into Eqs. 2.27 and 2.28 to find the fields $\mathbf{E}^{PE}$, $\mathbf{H}^{PE}$ for the polarized electric Gaussian beam.

To derive the PM solution we require a Gaussian field distribution for the magnetic field at the beam waist which yields the following spectrum

$$\hat{H}_y(k_x, k_y; 0) \;=\; H_o\,\frac{w_o^2}{2}\,\mathrm{e}^{-(k_x^2+k_y^2)\frac{w_o^2}{4}}, \tag{2.32}$$

Here, we chose $\mathbf{H}_o$ to point in y direction, i.e. $\mathbf{H}_o = H_o\,\mathbf{n}_y$. Similar to the case before, we insert the spectrum into Eqs. 2.29 and 2.30 to find the fields $\mathbf{E}^{PM}$, $\mathbf{H}^{PM}$ for the polarized magnetic Gaussian beam.

Although we found the generalized fields for a Gaussian beam, we are left with expressions with two infinite integrals that cannot be solved analytically. It is straight forward (see Section 2.7) to transform the integrals to cylindrical coordinates where it is possible to analytically integrate the angular dependence. This way we are left with a single, semi-infinite integral which has to be solved numerically. We avoid this procedure at this point since a rigorous description of a Gaussian beam is of limited practical importance. A Gaussian beam is generated in a confocal resonator with spherical end mirrors. Most resonators use slowly converging beams for which the paraxial approximation is sufficient. Furthermore, the field distribution near the focus of a strongly focused laser beam is determined by the boundary conditions of the focusing element such as a high f number lens. Therefore, the generalized Gaussian beams presented in this section are not adequate to describe the focal fields outside the laser cavity. But even for the case of a strongly converging confocal cavity we do not know how to superimpose the two independent PE and PM solutions. Barton and Alexander [4] use a an equal superposition but in principle any combination is a legitimate solution. In Section 2.6 we will present a formalism to accurately describe the focal fields of a strongly focused laser beam.

2.3.2 Higher order laser beams

The fields of the fundamental Gaussian mode can be used to derive higher order beam modes. The most commonly encountered higher beam modes are Hermite-Gaussian and Laguerre-Gaussian beams. The former are generated in cavities with rectangular end mirrors whereas the latter are observed in cavities having circular end mirrors. In the transverse plane, the fields of these modes extend over larger distances and have sign variations in the phase. Since the fundamental Gaussian mode is a solution of a linear homogeneous partial differential equation, namely the Helmholtz equation, any combinations of spatial derivatives of the fundamental mode are also solutions to the same differential equation. Zauderer [5] pointed

out, that Hermite-Gaussian modes $\mathbf{E}^H_{nm}$ can be generated from the fundamental mode $\mathbf{E}$ according to

$$\mathbf{E}^H_{nm}(x,y,z) \;=\; w_o^{n+m}\,\frac{\partial^n}{\partial x^n}\frac{\partial^m}{\partial y^m}\,\mathbf{E}(x,y,z)\;, \tag{2.33}$$

where n, m denote the order and degree of the beam. Laguerre-Gaussian modes $\mathbf{E}^L_{n,m}$ are derived in a similar way as

$$\mathbf{E}^L_{nm}(x,y,z) \;=\; k^n\,w_o^{2n+m}\,\mathrm{e}^{ikz}\;\;\frac{\partial^n}{\partial z^n}\Big(\frac{\partial}{\partial x}+i\frac{\partial}{\partial y}\Big)^m\,\big\{\mathbf{E}(x,y,z)\,\mathrm{e}^{-ikz}\big\}\quad. \tag{2.34}$$

Thus, once an accurate solution for the fundamental Gaussian mode is obtained, any higher order mode can be generated by simply applying Eqs. 2.33 and 2.34. It can be shown, that Laguerre-Gaussian modes can be generated as a superposition of a finite number of Hermite-Gaussian modes and vice versa. The two sets of modes are therefore not independent. Note that the parameter w_o only represents the beam waist for the Gaussian beam and that for higher order modes the amplitude E_o does not correspond to the field at the focal point. Fig. 2.4 shows the fields in the focal plane ($z=0$) for the first four Hermite-Gaussian modes. As indicated by the arrows, the polarizations of the individual maxima are either in phase

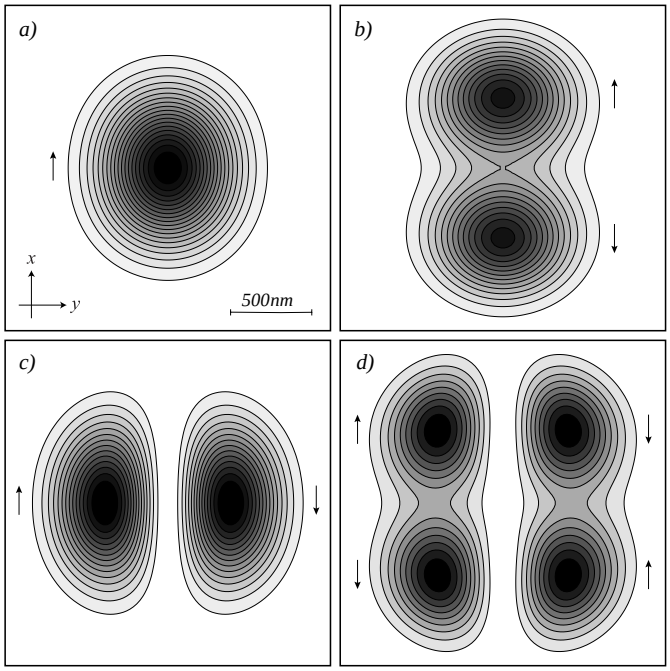

Figure 2.4: Intensity ($|\mathbf{E}|^2$) in the focal plane ($z=0$) of the first four Hermite-Gaussian modes. a) (00) mode (fundamental Gaussian mode), b) (10) mode, c) (01) mode, and d) (11) mode. The wavelength and beam angle are $\lambda=800nm$ and $\theta=28.65°$, respectively. The arrows indicate the polarization direction of the individual lobes. A linear scaling is used between contourlines.

or 180° out of phase with each other. The fields in Fig. 2.4 have been calculated beyond the paraxial approximation by an equal superposition of PE and PM solutions. As a consequence, the resulting fields of these beams possess longitudinal field components (E_z, H_z) as shown in Fig. 2.5 and Fig. 2.6. While the longitudinal electric field of the fundamental Gaussian beam is always zero on the optical axis it shows two lobes to the sides of the optical axis. Displayed on a cross-section through the beam waist, the two lobes are aligned along the polarization direction. The longitudinal electric field of the Hermite-Gaussian (10) mode, on the other hand, has it's maximum at the beam focus with a much larger field strength. This longitudinal field qualitatively follows from the 180° phase difference and the polarization of the two corresponding field maxima in Fig. 2.4, since the superposition of two similarly polarized plane waves propagating at angles $\pm\varphi$ to the z axis with 180° phase difference also leads to a longitudinal field component. It has been proposed to use the longitudinal fields of the Hermite-Gaussian (10) mode to accelerate charged particles along the beam axis in linear particle accelerators [6]. The longitudinal (10) field has also been applied to image the spatial orientation of molecular transition dipoles [7]. In general, the $(1,0)$ mode is important for all experiments which require the availability of a longitudinal field component. We shall see in Section 2.7 that the longitudinal field strength of a strongly focused higher order laser beam can even exceed the transverse field strength.

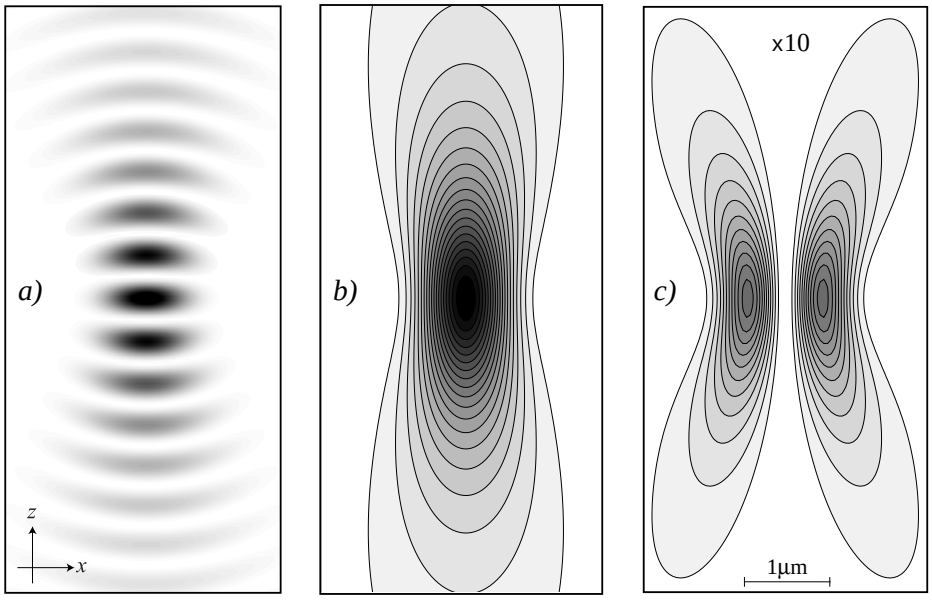

Figure 2.5: Fields of the fundamental Gaussian beam depicted in the polarization plane (x, z). The wavelength and beam angle are $\lambda = 800nm$ and $\theta = 28.65°$, respectively. a) Time dependent power density; b) Total electric field intensity ($|\mathbf{E}|^2$); c) Longitudinal electric field intensity ($|\mathbf{E}_z|^2$). A linear scaling is used between contourlines.

The commonly encountered doughnut modes with a circular intensity profile can be described by a superposition of Hermite-Gaussian or Laguerre-Gaussian modes. Linearly polarized doughnuts are simply defined by the fields $\mathbf{E}^L_{01}$ or $\mathbf{E}^L_{11}$. An azimuthally polarized doughnut mode is a superposition of two perpendicularly polarized $\mathbf{E}^H_{01}$ fields and a radially polarized doughnut mode is a superposition of two perpendicularly polarized $\mathbf{E}^H_{10}$ fields.

2.4 Angular spectrum representation of a dipole

Strongly localized sources such as dipoles are most conveniently described in a spherical coordinate system. The corresponding solutions of the wave equation are called multipoles. In order to couple these solutions with the angular spectrum picture we need to express the localized sources in terms of plane waves and evanescent waves. Let us start with the vector potential $\mathbf{A}$ of an oscillating dipole with its axis aligned along an arbitrary z-axis. The vector potential can be expressed as a one-component vector field as (see section ??)

$$\mathbf{A}(x,y,z) \;=\; A(x,y,z)\,\mathbf{n}_z \;=\; \frac{-ikZ_{\mu\varepsilon}}{4\pi}\,\frac{\mathrm{e}^{ik\sqrt{x^2+y^2+z^2}}}{\sqrt{x^2+y^2+z^2}}\,\mathbf{n}_z\;, \tag{2.35}$$

where $Z_{\mu\varepsilon}$ is the wave impedance of the medium. Besides a constant factor, the expression on the right hand side corresponds to the scalar Green's function (c.f. Eq. ??). According

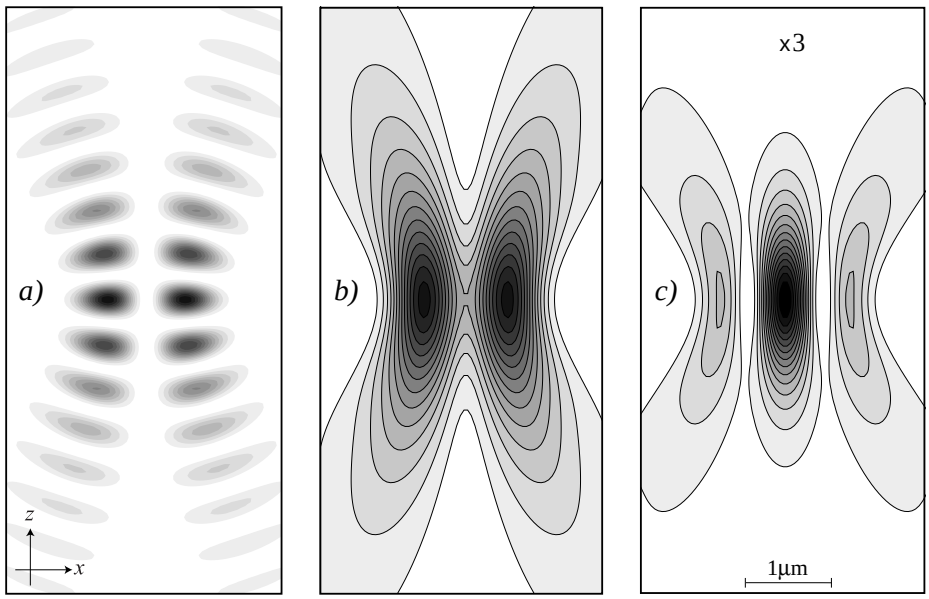

Figure 2.6: Fields of the Hermite-Gaussian (10) mode. Same scaling and definitions as in Fig. 2.5.

to Eq. ?? and Eq. ?? the electric and magnetic fields are obtained from $\mathbf{A}$ as

$$\mathbf{E}(x,y,z) = i\omega\,(1+\frac{1}{k^2}\nabla\nabla\cdot)\,\mathbf{A}(x,y,z) \tag{2.36}$$

$$\mathbf{H}(x,y,z) = \frac{1}{\mu_o\mu}\,\nabla\times\mathbf{A}(x,y,z)\ . \tag{2.37}$$

Thus, the electromagnetic field of the dipole can be constructed from the function $\exp(ikr)/r$, where $r=(x^2+y^2+z^2)^{1/2}$ is the radial distance from the dipole's origin. To find an angular spectrum representation of the dipole's electric and magnetic field we need first to find the angular spectrum of the function $\exp(ikr)/r$. This is not a trivial task and cannot be derived with the framework we have established in Section 2.1. The reason is that the function $\exp(ikr)/r$ is singular at $r=0$ and therefore not divergence free at its origin. The homogeneous Helmholtz equation 2.3 which formed the basis for our angular spectrum representation is not valid in the present case. Nevertheless, using a more careful analysis combined with complex contour integration it is possible to derive an angular spectrum representation of the function $\exp(ikr)/r$. Since the derivation can be found in other textbooks [3, 9] we state here only the result which reads as

$$\frac{\mathrm{e}^{ik\sqrt{x^2+y^2+z^2}}}{\sqrt{x^2+y^2+z^2}} = \frac{i}{2\pi}\iint_{-\infty}^{\infty}\frac{\mathrm{e}^{ik_x x+ik_y y+ik_z|z|}}{k_z}\,dk_x\,dk_y\ , \tag{2.38}$$

where we require that the real and imaginary parts of k_z stay positive for all values of k_x, k_y in the integration. This equation is known as the Weyl identity [10].

2.5 Farfields in the Angular Spectrum Representation

Consider an optical field in the object plane $z=0$ with the angular spectrum representation

$$\mathbf{E}(x,y,z) = \frac{1}{2\pi}\iint_{-\infty}^{\infty}\hat{\mathbf{E}}(k_x,k_y;0)\ \mathrm{e}^{i\,[k_x x+k_y y\pm k_z z]}\,dk_x\,dk_y\ . \tag{2.39}$$

We are interested in the asymptotic far-zone approximation of this field, i.e. in the evaluation of the field in a point $\mathbf{r}=\mathbf{r}_\infty$ with infinite distance from the object plane. The dimensionless unit vector $\mathbf{s}$ in direction of $\mathbf{r}_\infty$ is given by

$$\mathbf{s} = (s_x,s_y,s_z) = (\frac{x}{r},\frac{y}{r},\frac{z}{r})\ , \tag{2.40}$$

where $r=(x^2+y^2+z^2)^{1/2}$ is the distance of $\mathbf{r}_\infty$ from the origin. To calculate the farfield $\mathbf{E}_\infty$ we require that $r\to\infty$ and rewrite Eq. 2.39 as

$$\mathbf{E}_\infty(s_x,s_y,s_z) = \lim_{kr\to\infty}\frac{1}{2\pi}\iint_{(k_x^2+k_y^2)\le k^2}\hat{\mathbf{E}}(k_x,k_y;0)\ \mathrm{e}^{ikr\,[\frac{k_x}{k}s_x+\frac{k_y}{k}s_y\pm\frac{k_z}{k}s_z]}\,dk_x\,dk_y\ . \tag{2.41}$$

Because of their exponential decay, evanescent waves do not contribute to the fields at infinity. We therefore rejected their contribution and reduced the integration range to $(k_x^2+k_y^2)<k^2$.

The asymptotic behavior of the double integral as $kr \to \infty$ can be evaluated by the method of *stationary phase*. For a clear outline of this method we refer the interested reader to chapter 3.3 of Ref. [3]. Without going into details, the result of Eq. 2.41 can be expressed as

$$\mathbf{E}_\infty(s_x, s_y, s_z) \;=\; -ik\, s_z\, \hat{\mathbf{E}}(ks_x, ks_y; 0)\, \frac{\mathrm{e}^{ikr}}{r}\;. \tag{2.42}$$

This equation tells us that the farfields are entirely defined by the Fourier spectrum of the fields $\hat{\mathbf{E}}(k_x, k_y; 0)$ in the object plane if we replace $k_x \to ks_x$ and $k_y \to ks_y$. This simply means that the unit vector $\mathbf{s}$ fulfills

$$\mathbf{s} = (s_x, s_y, s_z) = (\frac{k_x}{k}, \frac{k_y}{k}, \frac{k_z}{k})\;, \tag{2.43}$$

which implies that only one plane wave with the wavevector $\mathbf{k} = (k_x, k_y, k_z)$ of the angular spectrum at $z = 0$ contributes to the farfield at a point located in the direction of the unit vector $\mathbf{s}$. The effect of all other plane waves is canceled by destructive interference. Combining Eqs. 2.42 and 2.43 we can express the Fourier spectrum $\hat{\mathbf{E}}$ in terms of the farfield as

$$\boxed{\hat{\mathbf{E}}(k_x, k_y; 0) \;=\; \frac{ir\,\mathrm{e}^{-ikr}}{k_z}\,\mathbf{E}_\infty(k_x, k_y)} \tag{2.44}$$

This expression can be substituted into the angular spectrum representation (Eq. 2.39) as

$$\boxed{\mathbf{E}(x, y, z) \;=\; \frac{ir\,\mathrm{e}^{-ikr}}{2\pi} \iint\limits_{(k_x^2+k_y^2)\le k^2} \mathbf{E}_\infty(k_x, k_y)\;\mathrm{e}^{i[k_x x + k_y y \pm k_z z]}\;\frac{1}{k_z}\,dk_x\,dk_y} \tag{2.45}$$

Thus, as long as evanescent fields are not part of our system then the field $\mathbf{E}$ and its farfield $\mathbf{E}_\infty$ form essentially a Fourier transform pair. The only deviation is given by the factor $1/k_z$. In the approximation $k_z \approx k$, the two fields form a perfect Fourier transform pair. This is the limit of *Fourier optics*.

As an example consider the diffraction at a rectangular aperture with sides $2L_x$ and $2L_y$ in an infinitely thin conducting screen which we choose to be our object plane ($z = 0$). A plane wave illuminates the aperture at normal incidence from the back. For simplicity we assume that the field in the object plane has a constant field amplitude $\mathbf{E}_o$ whereas the screen blocks all the field outside of the aperture. The Fourier spectrum at $z=0$ is then

$$\begin{aligned}\hat{\mathbf{E}}(k_x, k_y; 0) \;&=\; \frac{\mathbf{E}_o}{2\pi}\int_{-L_y}^{+L_y}\int_{-L_x}^{+L_x}\mathrm{e}^{-i[k_x x' + k_y y']}\;dx'\,dy' \\ &=\; \mathbf{E}_o\,\frac{2L_xL_y}{\pi}\,\frac{\sin(k_x L_x)}{k_x L_x}\,\frac{\sin(k_y L_y)}{k_y L_y}\;,\end{aligned} \tag{2.46}$$

With Eq. 2.42 we now determine the farfield as

$$\mathbf{E}_\infty(s_x, s_y, s_z) \;=\; -ik\, s_z\,\mathbf{E}_o\,\frac{2L_xL_y}{\pi}\,\frac{\sin(ks_x L_x)}{ks_x L_x}\,\frac{\sin(ks_y L_y)}{ks_y L_y}\,\frac{\mathrm{e}^{ikr}}{r}\;, \tag{2.47}$$

which, in the paraxial limit $k_z \approx k$, agrees with Fraunhofer diffraction.

Eq. 2.42 is an important result. It links the near-fields of an optical problem with the corresponding farfields. While in the near-field a rigorous description of fields is necessary, the farfields are well approximated by the laws of geometrical optics.

2.6 Focal fields of tightly focused laser beams

The limit of classical light confinement is achieved with highly focused laser beams. Such beams are used in fluorescence spectroscopy to investigate molecular interactions in solutions [11] and the kinetics of single molecules on interfaces [12, 7]. Highly focused laser beams also play a key role in confocal microscopy, where resolutions on the order of $\lambda/4$ are achieved. In optical tweezers, focused laser beams are used to trap particles and to move and position them with high precision [13]. All these fields require a theoretical understanding of laser beams.

The fields of a focused laser beam are determined by the boundary conditions of the focusing optical element and the incident optical field. In this section we will study the focusing of a paraxial optical field by an aplanatic optical lens as shown in Fig. 2.7. In our theoretical treatment we will follow the theory established by Richards and Wolf [14, 15]. The fields near the optical lens can be formulated by the rules of geometrical optics. In this approximation the finiteness of the optical wavelength is neglected ($k \to \infty$) and the energy is transported along light rays. The average energy density is propagated with the velocity $v = c/n$ in direction perpendicular to the geometrical wavefronts. To describe an aplanatic lens we need two rules of geometrical optics: 1.) the sine condition and 2.) the intensity law. These rules are illustrated in Fig. 2.8. The *sine condition* states that each optical ray which emerges from or converges to the focus F of an aplanatic optical system intersects its conjugate ray on a sphere of radius f (Gaussian reference sphere), where f is the focal length of the lens. Under conjugate ray one understands the refracted or incident ray which

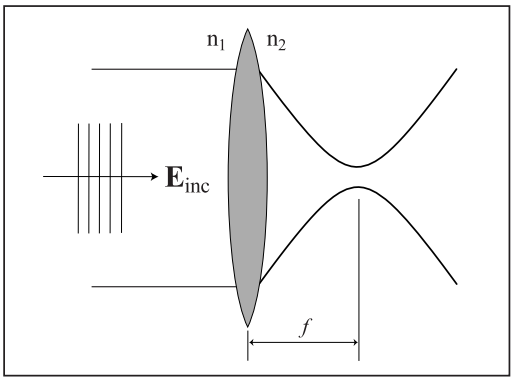

Figure 2.7: Focusing of a laser beam by an aplanatic lens.